SSRG International Journal of Civil Engineering
ISSN: 2348-8352/ https://doi.org/10.14445/23488352/IJCE-V13I2P120

Volume 13 Issue 2, 302-310, February 2026

Original Article

Performance Optimization of Conventional Savonius Rotor for Different Construction Materials through CFD Study

Amandeep Singh[1], Sonu Sharma[2]

[1,2]*Chitkara University Institute of Engineering and Technology, Chitkara University, Punjab, India*.

[1]*Corresponding Author : amandeep.cu484@chitkara.edu.in*

Received: 24 November 2025 Revised: 25 December 2025 Accepted: 26 January 2026 Published: 11 February 2026

Abstract *- The study concludes the potential for conducting a computational analysis on the conventional design of the Savonius rotor made with Poly-Lactic Acid (PLA), which is a 3-D printer material. This material can be molded into any shape with the 3D printer capabilities. The output from the simulation results thus provides an effective design solution for the purpose of constructing the Sovonius Rotor to be produced by a 3D printing technology. A computer design model thus aids in conducting simulation studies to find the torque and Coefficient of Performance (COP) as the primary performance indicators, followed by structural analysis on the rotor blades as the secondary performance indicator. It is a dual simulation study for the evaluation of torque based on the best design of the rotor, for the production of these designs based on the material selection after structural analysis simulation test, both conducted by ANSYS. The material selection was based on easily available metallic and composite material choices, such as aluminum, steel, and PLA. These materials were tested for their structural deformity under wind velocities of 6 m/s, 8 m/s, and 10 m/s. The COP was found to be maximum at 10 m/s for the configuration of the turbine used. The use of PLA is an affordable 3D printing material for building a small Vertical-Axis Wind Turbine (VAWT). PLA is a light material having low density and thermal conductivity as compared to steel and aluminum (88%), tested for producing stress values of 14 mPa, 156 mPa, and 10638 MPa, respectively, at 10 m/s. Deformation over rotor blades was found to be highest for aluminum (88%) at 1 m, and lowest for steel at 0.015 m. Though steel shows more reliable deformation results, PLA is a more preferred material for complex designs of 3-D printing turbine construction due to the lower material cost than steel.*

Keywords *- Horizontal Axis Wind Turbine, Vertical Axis Wind Turbine, Poly-Lactic Acid, Computer Aided Design, Computational Fluid Dynamics, Shear Stress Turbulence Model, Coefficient of Performance.*

1. Introduction

Wind energy is an essential source of non-conventional energy that can be harnessed to fulfill the demand for an increase in power consumption using a wind turbine. The utilization of freely available wind is a potential source from which energy can be generated. The energy can be produced through a device called a wind turbine. These are categorized according to their method of operation. Generally, the axis of rotation is considered for its operation. There is one turbine, which is most used, a Horizontal Axis Wind Turbine (HAWT), and another type, very rarely used, a Vertical Axis Wind Turbine (VAWT). The HAWTs are being adopted commercially than VAWTs in India, and thus this abandons the use of abundantly available wind as a potential resource. India's rising potential to produce energy from wind has seen vivid changes during the last few years. With more states participating, Tamil Nadu (10 GW), Gujarat (8.3 GW), Maharashtra (5 GW), Karnataka (4.9 GW), and Rajasthan (4.32 GW), there is a huge scope to produce energy on land [1]. Therefore, the effective utilization of all the freely available wind can be increased by making use of an omnidirectional turbine, which is classified as a vertical axis wind turbine called a Savonius rotor, as it is easier to construct, operate, and maintain, and requires low wind speeds to operate from any direction of the wind [2]. The researchers have tried to modify the conventional design of the vertical-axis wind turbine developed by S.J. Savonius. The research data shows modifications in the designs of conventional rotors through changes in geometry, configuration, or augmentation to extract more power. A lot of research work through experimentation was conducted over the past century. With the advent of modern science, experimentation has evolved to simulation and numerical solvers like ANSYS CFX. A solver uses pre-loaded mathematical equations and algorithms to redefine the geometries into newer prospects for research through which the newer designs can be optimized. The computer analysis involves replicating the actual geometry

into a Computer-Aided Design (CAD) model and then performing the simulation study, defined as a finite element analysis. This study inherits the concepts of physics to solve the momentum, conservation of energy, and mass equations on the working fluids [2]. To validate a new design, the output from the simulation is verified with the published data from the literature. Geometric changes in the overall physical structure of the rotor affect the performance of the rotor [3]. The use of external augmentation with the rotor design also plays a key role in increasing the efficiency of the rotor [4]. The selection of material is the last component, which is often ignored, as it plays a key role in finding the coefficient of torque [5]. There is a lot of published research on design modifications through external augmentation, but very little information is available on material selection and simpler designs [6]. There are rare studies that have analyzed the relation between blade material surface roughness and performance of the turbine through stresses and deformation for different surface roughness values at different velocities [7]. Studies have also been performed to improve the designs with an aim to manufacture a low-cost rotor from composite materials such as glass-polyester for dynamic parameters such as frequency, mode shape, and damping factor [8]. Table 1 shows research work accomplished in the past, which highlights the need for novelty and is brought into the current study.

1.1. Research Gap

The current study ensures the feasibility of producing a low-cost rotor by using the construction material, Poly-Lactic Acid (PLA) with 1 mm sheet thickness. This CAD model of the rotor was produced to find stress and deformation formed over the rotor blades for specific values of the input wind velocities. The validation of the rotor CAD model was done using the validated data from the literature for the value of the torque produced by the rotor, and then conducting the structural analysis of the model to identify the efficient material for the manufacturing of a Savonius rotor [9]. Steady state analysis using the Shear Stress Transport (SST) model is employed as the turbulence model in ANSYS CFX.

Table 1. Design parameters and output values obtained

Design Parameters	Conclusion and Output Values	Technique and Validation
Multiple quarter blade of rotor study, no change in overlap and aspect ratio [2]	Maximum performance coefficient of 0.2081 achieved at inlet velocity of 8.23 m/s, an 8.9% increase from the past value.	CFD Methodology, validated with Saha et al. (2008) wind tunnel experiments
Helical Blade for Savonius rotor, twist angle 45 to 90, overlap, aspect ratio, number of blades [3]	Smooth rotation & operational stability, a higher aspect ratio results in better performance coefficient. Composite materials are preferred over aluminum and steel.	3D CFD is preferred over 2D CFD because 2D overestimates the performance coefficient with SST k-w as the best suitable model.
Use of elliptical, Bach, Banesh, modified semicircular, slotted blades, maintaining overlap between 0.1 to 0.2 of end disk diameter and a higher aspect ratio [4]	Use of curtains, deflectors, guiding vanes, and end plates reduces losses in performance and prevents pressure equalization between advancing and returning blades. The performance coefficient lies between 0.15 and 0.35.	CFD, SST k-e, and k-w models were used.
Attention given to blade material induced inertia in the Savonius rotor design [5]	Polymeric materials produce better results than metallic blade materials due to higher mass and high torque requirements.	Structural deformation study to predict the results.
Scooplet-shaped blades, augmented with deflectors [6]	With 8 deflector, the best design gave a maximum performance coefficient of 0.35, and with 4 deflector, a material-efficient configuration gave maximum performance of 0.32.	CFD SST k-w, URANS

1.2. Model Under Analysis

There is limited published data on the use of blade materials through computational fluid dynamics studies. The common construction materials used for experimentation are aluminum. It is the most widely used material for rotor construction in experimentation. In this research, the first step is to produce a computer-generated model, which is prepared using any Computer-Aided Design (CAD) software. The model dimensions are taken from the experimental data [2], according to which the domain consists of two parts: the stator

and the rotor. The conventional Savonius rotor is in the form of two semicircular blades oriented together to form a circular shape. Many studies have supported computer-aided simulations instead of actual experimentations to lower the cost and prevent hazards while carrying out the work of research. It employs numerical simulations through software packages to carry out the entire calculations for the setup and experimentation [10]. For most computer simulations, the geometry of the rotor is designed by keeping a zero separation and a finite overlap between the two semicircular blades. These simulations can be performed on a revolving rotor through a transient approach and for a static rotor through a steady state approach through the available selection of the turbulence equations in the simulation software [11].

Table 2 tabulates the selection of the turbulence model from the ANSYS CFX solver. The selection of an appropriate turbulence model decides the nature of the simulation.

Table 2. Turbulence model selection based on area of application

RANS- Eddy Viscosity Models	RANS- Reynolds-Stress Models	Eddy Simulation Models
Zero Equation	SSG model	Large Eddy Simulation (LES)
Standard k-ε, k-ω model	LRR model	Detached Eddy Simulation (DES)
Shear Stress Transport (SST) model	BSL EARSM model	Scale Adaptive Simulation SST (SAS)
		Stress Blended Eddy Simulation

The selection of an appropriate turbulence model for the simulation depends on the cost and the time it will take to produce the desired results. Turbulence models based on Reynolds Averaged Navier Stokes (RANS) equations are less time-consuming and cost-effective. The use of the CFD approach has conveniently provided an advantage to understand the conditions of flow around the Savonius rotors [12]. The use of RANS for finding the results is most widely adopted. It is based on the laws of conservation of mass and momentum; thus, one of the supporting turbulence models that can be used is the Shear Stress Transport (SST) model in the current study.

The Shear Stress Turbulence (SST) model for the simulation was selected, which is a blend of k-ε and k-ω models; however, k-ε is used for far field, and k-ω is used for near wall calculations [2]. It consists of Reynolds Averaged Navier Stokes equations, which use the effect of the turbulence in the whole fluid continuum to predict the fluid behavior, near wall regions on the blade surface. The use of CFD is another sphere of science in which conditions are set up virtually to mimic the actual environment.

There are a few turbulent parameters that carry importance while conducting the simulation through ANSYS CFX.

- Friction Coefficient (C'_f): It measures the amount of interaction between two surfaces.
- Wall Shear Stress (τ_w): Tangential force per unit area that is exerted by the flowing fluid on the surface of the wind tunnel.
- Friction Velocity (u_t): A parameter that describes the velocity of flow in a stream, to the velocity that relates shear between layers in a fluid.
- Specific Dissipation Rate (ω): Rate at which the turbulent kinetic energy is converted into thermal internal Energy per unit volume and time.
- Turbulent Viscosity Ratio (β): Ratio of turbulent viscosity to the molecular viscosity.
- Turbulent Intensity (I): Intensity of wind velocity fluctuation.
- Turbulent Kinetic Energy (k): measured as root mean square in Reynolds Averaged Navier Stokes Equation.
- Turbulent Dissipation Rate (ε): Rate at which the turbulent kinetic energy is converted into thermal internal Energy.
- Reynolds Number (R_e): Used to determine if the fluid flow is turbulent or laminar

The calculation of the turbulent parameters is an important step towards the efficient use of the turbulence model. Acting fluid is air at 25^0 C with density (ρ) = 1.187 m^3. The intensity of the turbulence is often available in a low, medium, and high range of values. Table 3 shows the calculated values used as inputs for the turbulent parameters, which are often available in the sets to be used.

Table 3. Calculated turbulent parameters for the given geometry

u (m/s)	C'_f	τ_w (kg/ms^2)	I	k (m^2/s^2)	ε (m^2/s^3)	ω (s^{-1})	y_p (m)	u_t (m/s)
6	0.0054	0.11521	0.0361	0.07051	0.11731	18.4728	0.00004871	0.31151
8	0.0051	0.20331	0.0347	0.12262	0.26883	24.3571	0.00003682	0.41381
10	0.0048	0.29751	0.0338	0.17763	0.46862	29.3127	0.00003041	0.50073

1.3. Geometry Construction

Here, the design parameters have an overlap ratio (x) = 22 %, separation ratio (y) =0, aspect ratio (H/R) of 1.58, and the blades are vertical with end plate diameter (D) equal to 1.1 times the diameter of the rotor (d). The CAD model will first be meshed using

ANSYS CFX, after which the boundary conditions will be applied to simulate the results. The inlet velocities are taken at 6 m/s, 8 m/s, and 10 m/s. The fluid continuum is air at 25 °C, non-buoyant. The rotor produces an angular velocity (w) which can thus be calculated using 2πN/60. For the given rotor profile, Figure 1 describes the design characteristics thus considered in this study.

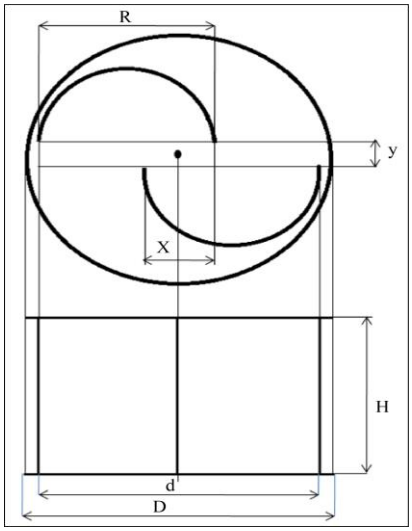

Fig. 1 CAD model developed for the analysis by ANSYS CFX

A geometry is prepared using a computer-aided design software by keeping the dimensions as close to the experimental model from the literature. In computational fluid analysis, the geometry needs to be divided into a small number of cells for the application of finite element analysis. This technique assists the use of three principal steps, starting from pre-processing, setup, and post-processing. One small cell represents the whole fluid continuum, and the solver integrates the sum of required values.

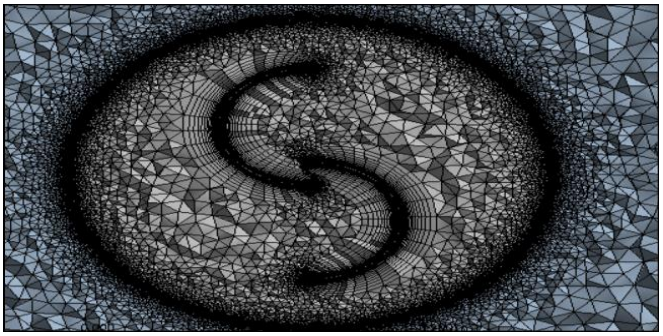

Fig. 2(a) Mesh generated by ANSYS within the domain of the stator and rotor

Figure 2(a) illustrates the mesh generated using the meshing module available within the CFX module on a larger scale, showing the stator domain and the rotor domain, whereas 2(b) shows the mesh generated with a value of y^+. The minimum requirement of meshing involves the allocation of the value of a boundary layer thickness (y^+), to be formed near the wall, often referred to as the boundary layer mesh, and as an important scope in this study to calculate the torque on the surface of the rotor blades.

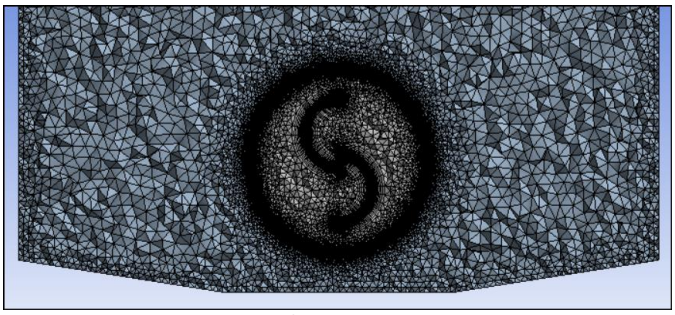

Fig. 2(b) Mesh generated with first layer thickness, y_p= 4.87e-05, and y+ = 1, layers formed over the blade's surface

After substantial meshing conditions, the discretized model is set up for the calculation of torque. Here, boundary conditions are applied by selecting the SST k-ω turbulence model in a steady state-frozen rotor approach. The working fluid is air at 25°C. The meshing involves the formation of elements and thus nodes by calculating the value of the boundary layer thickness (Yp). The boundary layer phenomenon illustrates the effects of turbulence close to the wall of the blade.

It lies in the viscous layer formed on the blade surface. Table 4 describes the formation of the number of elements and nodes for y+ equal to 1.

Table 4. Meshing obtained for Yp values at different inlet velocities (u)

Inlet Velocity (u) m/s	Yp
6	0.000048
8	0.000036
10	0.000030

2. Setup

The meshing is obtained for calculated values of boundary layer thickness for different wind velocities. Post meshing, the geometry is set up for testing, in which the boundary conditions are applied. The geometry consists of a stationary and a rotary domain. Therefore, appropriate values of input parameters are entered into the simulation software for defined boundary conditions. The most useful input parameters are listed as follows.

1. Inlet velocity
2. Working fluid
3. Direction of rotation

4. Angular velocity
5. Slip, no slip/free wall condition
6. Exiting conditions

The simulation run generates the values of outputs as the torque required from the rotor in the results module of the *ANSYS-CFX*. In addition to this, the quality of the mesh generated for an appropriate value of *Yp* is further studied through grid convergence. It is observed from the output values of torque that a better Coefficient Of Performance *(COP)* is calculated when the generated mesh is refined Table 5.

Table 5. Grid convergence study for Yp value

Inlet Velocity (u) m/s	Mesh Type	COP (SST k-ω model)
10	Coarse	0.154
10	Fine	0.183

3. Result and Discussion

The output values of the torque are used to calculate the Coefficient of Performance (COP). When values were compared with the experimental data, there were some notable differences seen for the obtained COP values in Table 6 and Figure 3, but the trend was similar.

Table 6. Calculated the COP experimental data and the COP model 1 at y+ = 1

Inlet Velocity (u) m/s	COP (experimental data)	Calculated COP (SST k-ω model)
6	0.072	0.167
8	0.178	0.199
10	0.106	0.179

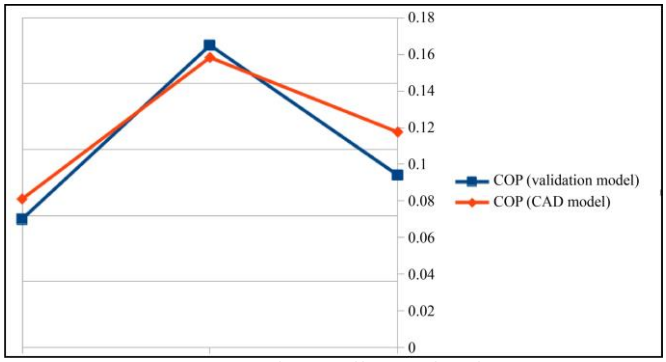

Fig. 3 Validation of the coefficient of performance

This result analysis validated the possibility for the simulation of conventional Savonius rotor geometry for any further design modification. A possible fact is that the modified designs can be simulated to find the optimum COP values and can be 3D printed for the actual energy harvesting.

The study is further expedited for the material selection through structural analysis for the same model under study for the total deformation and stresses produced. Figure 4 (a), (b), (c) illustrates the use of a two-dimensional (2D) geometry for carrying out a structural analysis test.

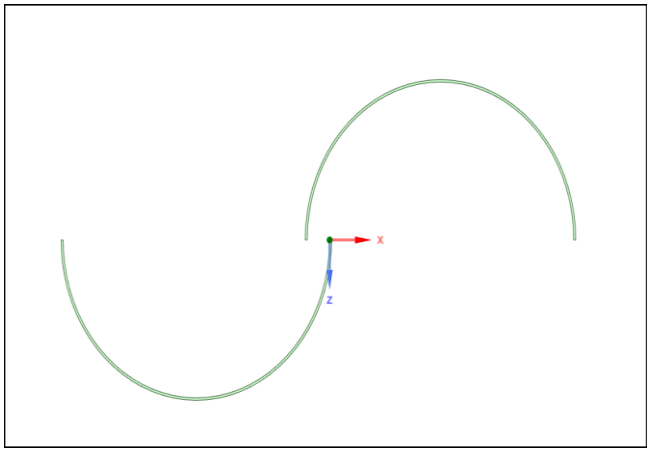

Fig. 4(a) Model under structural analysis

Figure 4 (b) is the two-dimensional model under study for maximum deformation. Figure 4(c) 2-D meshing performed on the model.

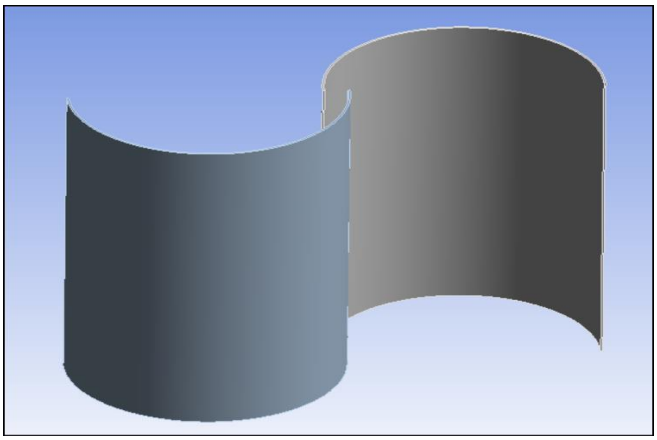

Fig. 4(b) Model under structural analysis, meshing for total deformation

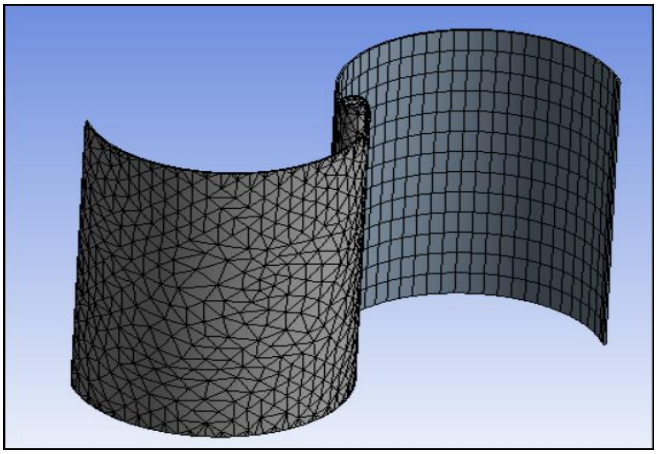

Fig. 4(c) Model under structural analysis, meshing for total deformation

A value comparison Table 6 lists material properties for three commonly available materials. Poly Lactic Acid (PLA) is the lightest material with the lowest value of density, which makes it a very suitable portable solution for easy installation in remote areas. It carries the lowest thermal conductivity, again making it suitable for energy production without affecting the ambient air temperature changes. It has the highest value of specific heat, making it a difficult choice to sustain heat on a hot day, but advancements consisting of providing a cooling system can be used, making it the best material choice for the construction of complex designs.

Table 7. Material properties

	Structural Steel	Alumina, 88%	PLA
Density (kg/m^3)	7850	3475	1140
Thermal Conductivity (W/m^{0}C)	60.5	13.74	0.243
Specific Heat (J/kg^{0}C)	434	768.6	1520

The deformation and equivalent stress tests are conducted for three materials. While it is to be noticed in Table 8 that structural steel has the lowest deformation, if considered to operate under varying wind velocities of 6 m/s, 8 m/s, and 10 m/s. Alumina also deforms earlier than PLA.

Table 8. Maximum deformation at 6 m/s, 8 m/s, and 10 m/s

Inlet Velocity (u) m/s	Structural Steel (m)	Alumina, 88%	PLA (m)
6	0.0065083	0.40965 m	0.06963
8	0.014903	0.93742 m	0.15934
10	0.015973	1.0054 m	0.17089

The stress values indicate the failure of the design under loading conditions, Table 9. Here, these values gives us the choice of consideration to be preferred for the actual model construction.

Table 9. Maximum equivalent stress (von-Mises) at 6 m/s, 8 m/s & 10 m/s

Inlet Velocity (u) m/s	Structural Steel	Alumina, 88%	PLA
6	63 mPa	4334 mPa	5.71 mPa
8	145 mPa	9919 mPa	13 mPa
10	156 mPa	10638 mPa	14 mPa

3.1. Total Deformation

Observed values from Table 9 show that the structural steel has the lowest deformation among alumina and PLA, and PLA has the lowest stresses formed on its surfaces than structural steel and alumina at rotational velocities of 40.84 rad/s, 61.78 rad/s, and 63.98 rad/s. Thus, Figure 5 shows the maximum deformation, and Figure 7 shows the maximum equivalent stress for alumina at three inlet wind velocities.

3.1.1. Alumina

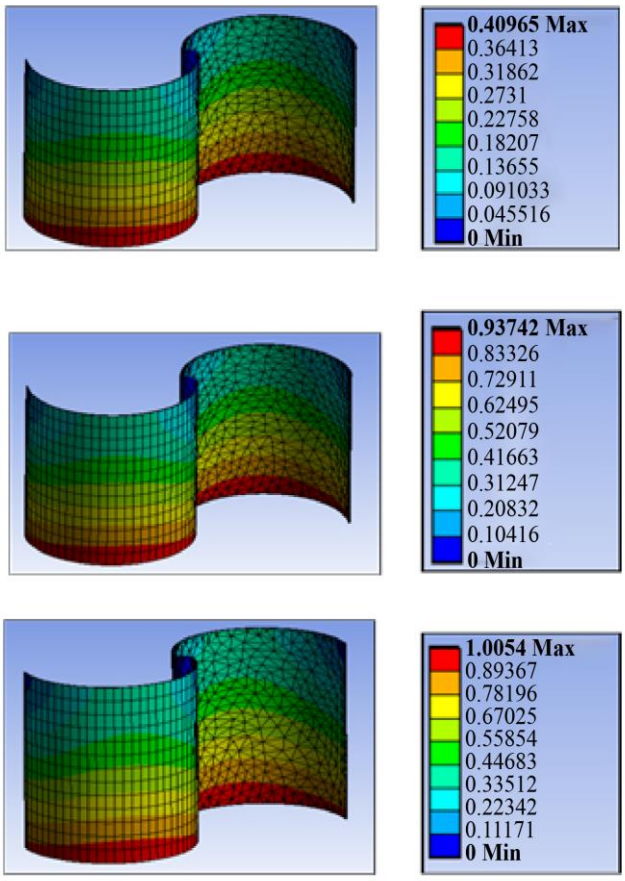

Fig. 5 Maximum deformation at 6 m/s, 8 m/s, and 10 m/s

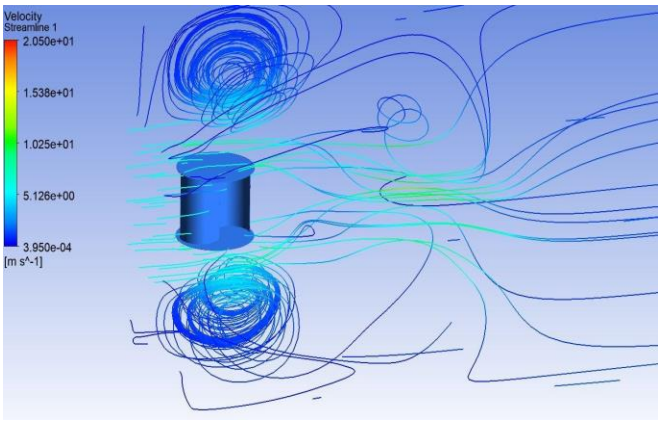

Fig. 6 Wind flow visualization over the rotor under analysis at u=6 m/s

3.2. Equivalent Stress

PLA has the lowest stresses formed on its surfaces than structural steel and alumina at rotational velocities of 40.84 rad/s, 61.78 rad/s, and 63.98 rad/s.

3.2.1. Alumina

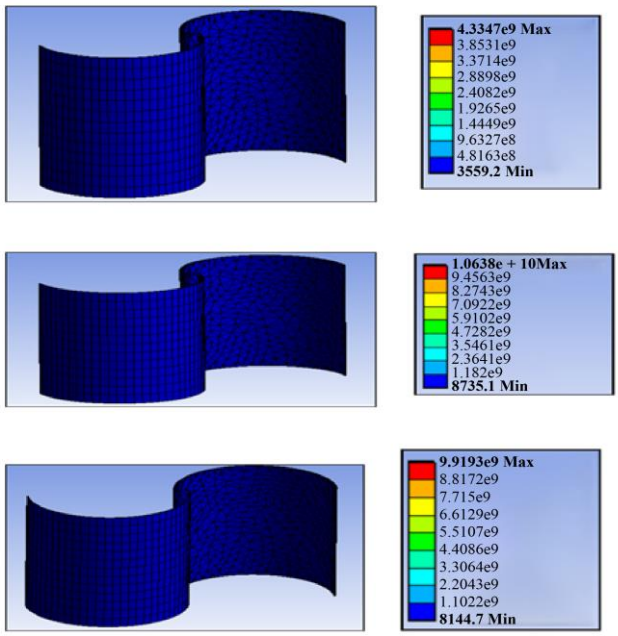

Fig. 7 Maximum equivalent stress at 6 m/s, 8 m/s, and 10 m/s

3.3. Pressure

The pressure distribution over the rotor blades was also released, showing significant formation of pressure zones at four fixed positions in the direction of flow. Here, the wind flow direction is kept fixed for testing purposes. The concave side of the blade acts as a dominator for the drag forces to produce positive torque, and the convex side of the blade produces a negative torque. The computed average torque value does produce the relevant desired effect and thus a COP close to the conventional model under testing.

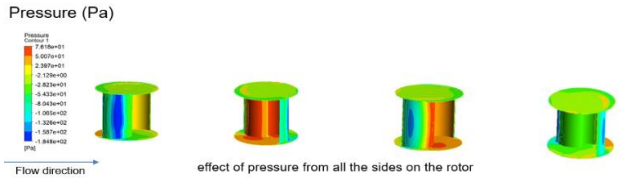

Fig. 8 Pressure captured in the stationary frame

Velocity contouring is thus studied as a measure of flow visualization over the entire continuum, as in Figure 6. It is clearly seen in Figure 8 that the flow around the rotor is turbulent. The wind velocity at the tunnel exit is 6 m/s, while in Figure 9, the velocity changes are captured in a stationary frame at four fixed positions. The velocity is in the provided range on the concave side of the blade, while it is reduced on the convex side of the blade for the conventional Savonius rotor.

These are only essential input parameters that are often overlooked while designing the geometry for the rotor. A rotor design thus must be simple in construction to be able to work with available wind velocities to predict a similar trend and produce efficient results with computational analysis.

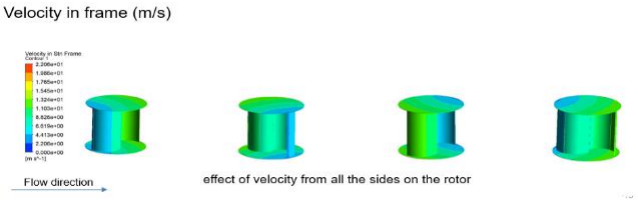

Fig. 9 Velocity behavior captured in the stationary frame

The CFD, thus, is an effective method to produce and simulate the performance of the prototypes for several modified models conditioned under virtual environmental conditions, and is a cost-effective method for conducting the analysis.

4. Conclusion

The validated results establish the unique feasibility of this technique. The results state the closest approximations to find the Coefficient of Performance (COP) for the conventional rotor. Thus, modified geometries can therefore be tested through this technique to improve the outputs and produce more efficient single-stage two-blade Savonius rotors.

For the practical feasibility of the ongoing analysis, a small-scale prototype has been constructed with the use of the CAD model and readily available 3D printing solutions. Poly-Lactic Acid (PLA), a bioproduct, has been used to produce the model, which is lighter, easily available as a bioproduct, biodegradable, and environmentally friendly, and is used as the most common material in 3D printing with deformation and stresses.

Fig. 10 A small-scale 3D printed model of the Savonius rotor by Poly-Lactic Acid (PLA)

References

[1] Abhishek Kumar et al., "An Overview of Wind Energy Development and Policy Initiatives in India," *Clean Technologies and Environmental Policy*, vol. 24, no. 5, pp. 1337-1358, 2022. [CrossRef] [Google Scholar] [Publisher Link]

[2] Sonu Sharma, and Rajesh Kumar Sharma, "Performance Improvement of Savonius Rotor using Multiple Quarter Blades-A CFD Investigation," *Energy Conversion and Management*, vol. 127, pp. 43-54, 2016. [CrossRef] [Google Scholar] [Publisher Link]

[3] Pinku Debnath, and V. Gandhirajan, "A Comprehensive Review on Design and Development Analysis and Blade Material Selection of Helical Savonius Rotor," *Wind Engineering*, vol. 47, no. 4, pp. 883-894, 2023. [CrossRef] [Google Scholar] [Publisher Link]

[4] Anupam Dewan, Adesh Gautam, and Rahul Goyal, "Savonius Wind Turbines: A Review of Recent Advances in Design and Performance Enhancements," *Materialstoday: Proceedings*, vol. 47, pp. 2976-2983, 2021. [CrossRef] [Google Scholar] [Publisher Link]

[5] M. Syukri. M. Shamsuddin, Noorfazreena M. Kamaruddin, and Zulfaa Mohamed-Kassim, "The Influence of Material on the Power Performance of Savonius Turbines in Wind and Water Applications," *Ocean Engineering*, vol. 266, 2022. [CrossRef] [Google Scholar] [Publisher Link]

[6] Ivo Marinić-Kragić, Damir Vučina, and Zoran Milas, "Robust Optimization of Savonius-Type Wind Turbine Deflector Blades Considering Wind Direction Sensitivity and Production Material Decrease," *Renewable Energy*, vol. 192, pp. 150-163, 2022. [CrossRef] [Google Scholar] [Publisher Link]

[7] Muhamad Hasfanizam Mat Yazik et al., "Effect of Surface Roughness and Blade Material on the Performance of a Stationary Savonius Wind Turbine under Different Operating Conditions," *Physics of Fluids*, vol. 35, no. 3, 2023. [CrossRef] [Google Scholar] [Publisher Link]

[8] Sobhy M. Ghoneam, Ahmed A. Hamada, and Taha S. Sherif, "Dynamic Analysis of the Optimized Savonius Vertical Axis Wind Turbine Composite Blades," *Journal of Solar Energy Engineering*, vol. 143, no. 5, 2021. [CrossRef] [Google Scholar] [Publisher Link]

[9] Petar Škvorc, and Hrvoje Kozmar, "Wind Energy Harnessing on Tall Buildings in Urban Environments," *Renewable and Sustainable Energy Reviews*, vol. 152, 2021. [CrossRef] [Google Scholar] [Publisher Link]

[10] Sukanta Roy, and Ujjwal K. Saha, "Review on the Numerical Investigations into the Design and Development of Savonius Wind Rotors," *Renewable and Sustainable Energy Reviews*, vol. 24, pp. 73-83, 2013. [CrossRef] [Google Scholar] [Publisher Link]

[11] M.H. Nasef et al., "Evaluation of Savonius Rotor Performance: Static and Dynamic Studies," *Journal of Wind Engineering and Industrial Aerodynamics*, vol. 123, pp. 1-11, 2013. [CrossRef] [Google Scholar] [Publisher Link]

[12] Anupam Dewan et al., "Computational Fluid Dynamics and Turbulence Modelling in Various Blades of Savonius Turbines for Wind and Hydro Energy: Progress and Perspectives," *Ocean Engineering*, vol. 283, 2023. [CrossRef] [Google Scholar] [Publisher Link]

[13] A.J. Alexander, and B.P. Holownia, "Wind Tunnel Tests on a Savonius Rotor," *Journal of Wind Engineering and Industrial Aerodynamics*, vol. 3, no. 4, pp. 343-351, 1978. [CrossRef] [Google Scholar] [Publisher Link]

[14] Hermann Schlichting, and Klaus Gersten, *Boundary-Layer Theory*, 9th ed., Springer Berlin, Heidelberg, 2017. [CrossRef] [Google Scholar] [Publisher Link]

[15] P.D. Fleming, and S.D. Probert, "A Proposed, Three-Sail, Savonius-Type Wind-Rotor," *Applied Energy*, vol. 12, no. 4, pp. 327-331, 1982. [CrossRef] [Google Scholar] [Publisher Link]

[16] S.A. Tabassum, and S.D. Probert, "Vertical-Axis Wind Turbine: A Modified Design," *Applied Energy*, vol. 28, no. 1, pp. 59-67, 1987. [CrossRef] [Google Scholar] [Publisher Link]

[17] T. Ogawa, H. Yoshida, and Y. Yokota, "Development of Rotational Speed Control Systems for a Savonius-Type Wind Turbine," *Journal of Fluids Engineering*, vol. 111, no. 1, pp. 53-58, 1989. [CrossRef] [Google Scholar] [Publisher Link]

[18] Nobuyuki Fujisawa, "On the Torque Mechanism of Savonius Rotors," *Journal of Wind Engineering and Industrial Aerodynamics*, vol. 40, no. 3, pp. 277-292, 1992. [CrossRef] [Google Scholar] [Publisher Link]

[19] Ujjwal K. Saha, S. Thotla, and Damodar Maity, "Optimum Design Configuration of Savonius Rotor through Wind Tunnel Experiments," *Journal of Wind Engineering and Industrial Aerodynamics*, vol. 96, no. 8-9, pp. 1359-1375, 2008. [CrossRef] [Google Scholar] [Publisher Link]

[20] Mohamed H. Mohamed et al., "Optimal Blade Shape of a Modified Savonius Turbine using an Obstacle Shielding the Returning Blade," *Energy Conversion and Management*, vol. 52, no. 1, pp. 236-242, 2011. [CrossRef] [Google Scholar] [Publisher Link]

[21] A. Dragomirescu, "Performance Assessment of a Small Wind Turbine with Crossflow Runner by Numerical Simulations," *Renewable Energy*, vol. 36, no. 3, pp. 957-965, 2011. [CrossRef] [Google Scholar] [Publisher Link]

[22] João Vicente Akwa, Horácio Antonio Vielmo, and Adriane Prisco Petry, "A Review on the Performance of Savonius Wind Turbines," *Renewable and Sustainable Energy Reviews*, vol. 16, no. 5, pp. 3054-3064, 2012. [CrossRef] [Google Scholar] [Publisher Link]

[23] A.R. Coughtrie, D.J. Borman, and Andrew Sleigh, "Effects of Turbulence Modelling on Prediction of Flow Characteristics in a Bench-Scale Anaerobic Gas-Lift Digester," *Bioresource Technology*, vol. 138, pp. 297-306, 2013. [CrossRef] [Google Scholar] [Publisher Link]

[24] Tong Zhou, and Dietmar Rempfer, "Numerical Study of Detailed Flow Field and Performance of Savonius Wind Turbines," *Renewable Energy*, vol. 51, pp. 373-381, 2013. [CrossRef] [Google Scholar] [Publisher Link]

[25] Konrad Kacprzak, Grzegorz Liskiewicz, and Krzysztof Sobczak, "Numerical Investigation of Conventional and Modified Savonius Wind Turbines," *Renewable Energy*, vol. 60, pp. 578-585, 2013. [CrossRef] [Google Scholar] [Publisher Link]

[26] Ida Bagus Alit et al., "Effect of Concentrator, Blade Diameter and Blade Number on the Savonius Wind Turbine Performance," *Asian Journal of Applied Sciences*, vol. 5, no. 2, pp. 343-351, 2017. [Google Scholar]

[27] A. Damak, Zied Driss, and Mohamed Salah Abid, "Optimization of the Helical Savonius Rotor through Wind Tunnel Experiments," *Journal of Wind Engineering and Industrial Aerodynamics*, vol. 174, pp. 80-93, 2018. [CrossRef] [Google Scholar] [Publisher Link]

[28] Nur Alom, and Ujjwal K. Saha, "Evolution and Progress in the Development of Savonius Wind Turbine Rotor Blade Profiles and Shapes," *Journal of Solar Energy Engineering*, vol. 141, no. 3, 2019. [CrossRef] [Google Scholar] [Publisher Link]

[29] A.M. Siregar, and C.A. Siregar, "Reliability Test Prototype Wind Turbine Savonius Type Helical as an Alternative Electricity Generator," *IOP Conference Series: Materials Science and Engineering*, vol. 674, no. 1, pp. 1-7, 2019. [CrossRef] [Google Scholar] [Publisher Link]

[30] W.A. El-Askary et al., "Experimental and Theoretical Studies for Improving the Performance of a Modified Shape Savonius Wind Turbine," *Journal of Energy Resources Technology*, vol. 142, no. 12, 2020. [CrossRef] [Google Scholar] [Publisher Link]

[31] A. Ciocănea et al., "Experimental Research on Increasing the Static Torque for a Small Savonius Rotor of Helical Type," *IOP Conference Series: Earth and Environmental Science*, *The 7th Conference of the Sustainable Solutions for Energy and Environment*, Bucharest, Romania, vol. 664, no. 1, pp. 1-8, 2021. [CrossRef] [Google Scholar] [Publisher Link]

[32] CFX Reference Guide, ANSYS Inc, 2026. [Online]. Available: https://ansyshelp.ansys.com/public/account/secured?returnurl=/Views/Secured/corp/v251/en/cfx_ref/cfx_ref.html